Solution structure of a viral DNA polymerase X and evidence for a mutagenic function

Alexander K. Showalter[1], In-Ja L. Byeon[2], Mei-I Su[1] and Ming-Daw Tsai[1–4]

[1]Department of Chemistry, [2]The Campus Chemical Instrument Center, [3]Department of Biochemistry and [4]The Ohio State Biochemistry Program, The Ohio State University, Columbus, Ohio 43210, USA.

The African swine fever virus DNA polymerase X (ASFV Pol X or Pol X), the smallest known nucleotide polymerase, has recently been reported to be an extremely low fidelity polymerase that may be involved in strategic mutagenesis of the viral genome. Here we report the solution structure of Pol X. The structure, unique within the realm of nucleotide polymerases, consists of only palm and fingers subdomains. Despite the absence of a thumb subdomain, which is important for DNA binding in other polymerases, we show that Pol X binds DNA with very high affinity. Further structural analyses suggest a novel mode of DNA binding that may contribute to low fidelity synthesis. We also demonstrate that the ASFV DNA ligase is a low fidelity ligase capable of sealing a nick that contains a G-G mismatch. This supports the hypothesis of a virus-encoded, mutagenic base excision repair pathway consisting of a tandem Pol X/ligase mutator.

A number of DNA polymerases have recently been described that copy template DNA with very low fidelity. The biological relevance of this error-prone activity, however, remains uncertain. Among the more extreme examples of an error-prone polymerase is African swine fever virus DNA polymerase X (ASFV Pol X). Pol X is the only polymerase that catalyzes nucleotide mispair formation with comparable efficiency to that with which it catalyzes formation of all four Watson-Crick base pairs[1]. It is also the only known extreme low fidelity polymerase encoded by a virus. On the basis of such properties, Pol X has been postulated to function as a strategic DNA mutase, promoting viral hypervariability *via* low fidelity synthesis[1].

Mammalian DNA polymerase β (Pol β), the known protein with the highest sequence homology to Pol X, functions in base excision repair (BER)[2]. The last step of BER is sealing of the newly synthesized, repaired strand into the genome by a DNA ligase. Based on its sequence homology to Pol β[3] and an apparent gap-filling functionality[1,4], Pol X is believed to participate in a viral BER pathway. This, in addition to the observations outlined above, led to the proposal that viral BER is mutagenic, driven by the error-prone activity of Pol X[1].

Here we report the structure of Pol X. In addition, a unique tolerance of the bulky G-G mismatch by ASFV DNA ligase is demonstrated, consistent with the hypothesis of a mutagenic viral BER pathway.

Structure of Pol X

The structure of Pol X was determined by heteronuclear NMR methods by assigning >97% backbone and >85% side chain resonances, and by simulated-annealing calculations using a total of 2,597 NMR-derived restraints. The structure is well defined

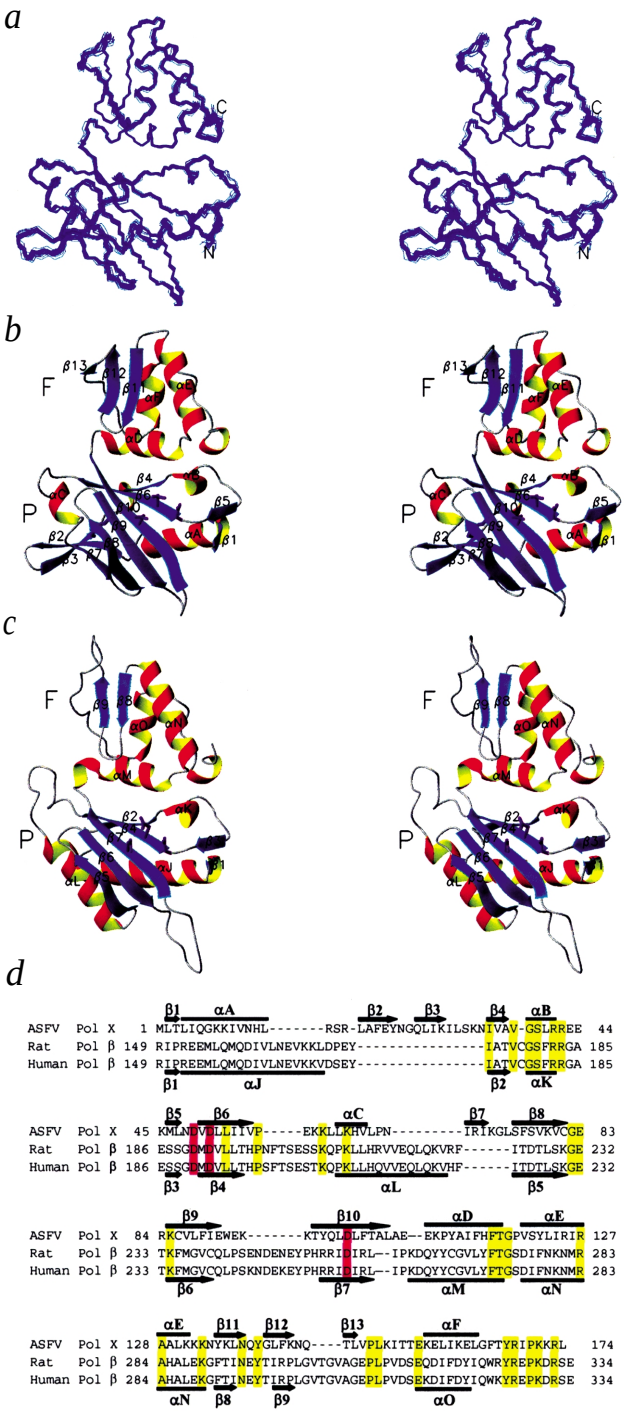

Fig. 1 NMR solution structure of Pol X and structural comparison with Pol β. ***a***, Backbone traces of the ensemble of 20 simulated annealing (SA) structures of Pol X. ***b***, Ribbon diagram of Pol X with secondary structural elements. The minimized mean structure is used. The side chains of the catalytic Asp triad are shown in purple, and the disulfide bond is in dark blue. ***c***, Ribbon diagram of Pol β with secondary structural elements and with the 8 kDa domain and thumb subdomain omitted (adapted from PDB code 1BPB). The side chains of the catalytic Asp triad are shown in purple. ***d***, Structure-based sequence alignment of Pol X with the palm and fingers subdomains of Pol β. Secondary structural elements as defined by the NMR structure of Pol X are shown above the alignment, and those by the crystal structure of Pol β (PDB code 1BPB) are shown below. Identical residues are labeled in yellow, and the catalytic Asp triads are labeled in purple. In all structural figures, the letters 'F', 'P' and 'T' refer to the fingers, palm and thumb subdomain, respectively.

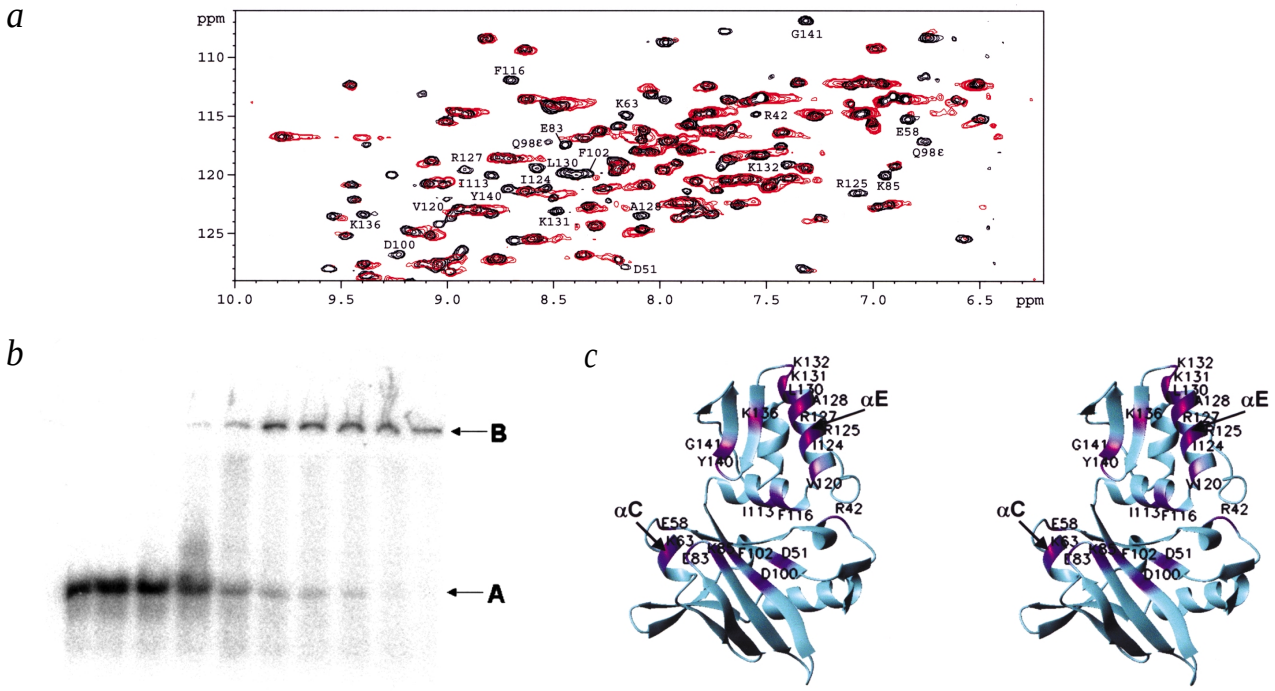

Fig. 2 Mapped DNA binding site of Pol X. ***a***, Superimposed ^{15}N-HSQC spectra of free Pol X (black) and Pol X in complex with gapped DNA (red). The peaks that initially undergo chemical shift change when gapped DNA is added ([Pol X]:[DNA] = 1:0.3) and eventually disappear at higher DNA concentrations (red; [Pol X]:[DNA] = 1:1) are labeled with sequence numbers. ***b***, Band shift assay showing binding of Pol X to the gapped DNA used in (*a*). Pol X concentration is, from left-to-right: 0, 0.1, 0.2, 0.4, 0.8, 1.6, 3.2, 6.4, 12.8 and 25.6 μM. Binding is observed as disappearance of free DNA (band A) and appearance of bound DNA (band B). ***c***, Pol X residues in the DNA binding site, as mapped by HSQC NMR experiments in (*a*), are colored purple in the ribbon diagram of Pol X.

(Table 1; Fig. 1*a*). As suggested by the ~55% sequence homology to the C-terminal half of Pol β, the structure of Pol X closely resembles that of the fingers and palm subdomains of Pol β[5] (Fig. 1*b–d*). The palm, fingers and thumb nomenclature, which was devised as a descriptive analogy to a human hand 'grasping' the DNA substrate[6], has been contested in terms of its application to Pol β. We prefer, for reasons described[7], the less frequently used application suggested by Steitz *et al.*[8] The difference between the two is simply a reversal of the names 'thumb' and 'fingers' for the subdomains on either side of the palm. A DALI search[9] of the protein databank shows that Pol X is structurally very similar to Pol β (PDB code 1BPB), with a Z score = 17.4 and a root mean square (r.m.s.) deviation = 2.3 Å for the backbone N, Cα and C′ atoms of 164 aligned residues. One *cis*-peptide bond is identified in Pol X (between Gly 118 and Pro 119) by a NOE pattern characteristic of a prolyl *cis*-peptide. The conserved *cis*-bond makes a sharp kink between helices αD and αE in Pol X, similar to the one between αM and αN in Pol β[10]. The active site carboxylate triad (Asp 49, 51 and 100) of Pol X is almost superimposable with that (Asp 190, 192 and 256) of Pol β (r.m.s. deviation is 0.90 Å for heavy atoms), indicating a general structural conservation of the active site.

However, significant differences in structural alignments are observed elsewhere. Pol X residues 18–28 form a β-hairpin (strands β2 and β3) that interacts with residues 69–71 (β7) to form a three-stranded β-sheet, whereas the corresponding regions in Pol β are α-helical. This novel three-stranded β-sheet truncates helices αA and αC, in the palm subdomain, relative to the homologous αJ and αL in Pol β. Other differences are observed in several loop regions. The three major loops in Pol β (between β4–αL and β6–β7 in the palm, and β8–β9 in the fingers) correspond to tight turns in Pol X, resulting in a slightly more compact structure. The loop following β9 in Pol β adopts a β-strand in Pol X (β13) to form a three-stranded β-sheet in the fingers. A disulfide bond was also identified between Cys 81(in β8) and Cys 86 (in β9) of Pol X (Fig. 1*b*) on the basis of the extremely down-field shifted ^{13}Cβ chemical shifts (47.6 and 50.6 p.p.m. for Cys 81 and 86, respectively)[11].

Under the conditions of our NMR studies, dithiothreitol (DTT) could not readily reduce the disulfide bond. Preliminary kinetic analysis indicates that the effects of DTT on the activity and fidelity are smaller than five-fold. The kinetic data reported were obtained in the presence of 1 mM DTT[1]. Whether the disulfide bond is present *in vivo* remains to be established. The fact that DNA viruses possess a conserved oxidoreductase system geared toward the maintenance of cytoplasmic disulfides[12] suggests that this disulfide bond might be a biologically relevant structural feature of Pol X. No crystal structure of Pol β shows a disulfide bond.

DNA Binding by Pol X

Crystal structures of a variety of polymerase–DNA complexes indicate that the thumb subdomain is extensively involved in DNA binding[10,13,14]. Likewise, analysis of tryptic fragments of Pol β has demonstrated that the ground state DNA binding function is localized entirely within the N-terminal 8 kDa domain and thumb subdomain[15] – structural motifs that are absent in Pol X. However, Pol X binds to gapped DNA at least as tightly as does native Pol β. Mutliple repetitions of titrations of Pol β and Pol X with gapped DNA, as monitored by pre-steady state burst amplitudes, yielded average $K_{d,DNA}$ values of 6 and 3 nM for Pol β and Pol X, respectively (data not shown). In addi-

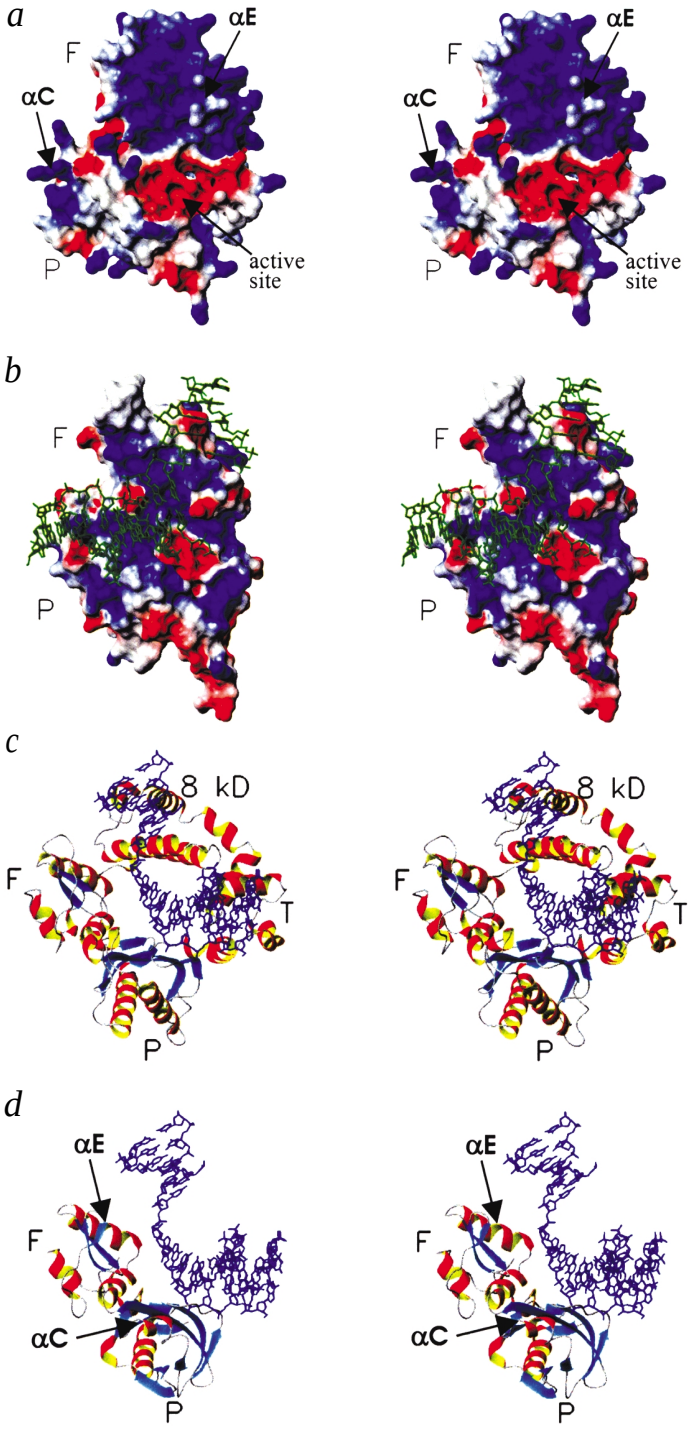

Fig. 3 Comparison of DNA Binding by Pol X and Pol β. ***a***, Surface representation of free Pol X. ***b***, Surface representation of Pol β (palm and fingers subdomains) bound to gapped DNA and an incoming nucleotide (adapted from PDB file 1BPY). In (*a*,*b*), blue and red indicate positive and negative charges, respectively. ***c***, Side view of the ribbon diagram of a Pol β–DNA complex (adapted from 1BPX). ***d***, The Pol X solution structure in the same orientation as Pol β in (*c*), with DNA from (*c*) superimposed relative to the carboxylate triad.

tion, a competition experiment in which Pol X and Pol β vie for limiting DNA substrate supports the conclusion that Pol X has a slightly higher DNA binding affinity than does Pol β (data not shown).

The origin of the potent DNA binding affinity of Pol X was examined by binding site mapping *via* ^{15}N-HSQC experiments (Fig. 2*a*). To ensure that the small DNA fragment used for NMR studies was stably bound by Pol X, a band shift assay was employed (Fig. 2*b*). The Pol X residues whose resonances are significantly perturbed by addition of gapped DNA run from helix αC in the palm subdomain to the catalytic carboxylate triad and then up the fingers subdomain (Fig. 2*c*). A surface electrostatic potential (Fig. 3*a*) shows that the mapped binding site contains an electropositive pocket surrounded by a hydrophobic wall in the fingers, as well as a number of electropositive residues in the palm. The binding pocket and outer wall of the fingers subdomain of Pol X are much more electropositive than the corresponding regions of Pol β — for example, Lys 131 and Lys 136 in Pol X replace Leu 287 and Thr 292 in Pol β — perhaps accounting in part for the DNA binding affinity of Pol X. The contour of the mapped DNA binding site in Pol X (Fig. 2*c*) is morphologically similar to the 'kinked' conformation of gapped DNA in complex with Pol β[16] (Fig. 3*b*), suggesting that the mapped residues interact with DNA to produce a similarly kinked conformation. The 8 kD domain and thumb subdomain of Pol β are mainly responsible for binding DNA (Fig. 3*c*), which has little contact with the fingers, in the kinked conformation[16]. When this DNA is superimposed relative to the catalytic carboxylate triad of Pol X (Fig. 3*d*), some alterations in the DNA conformation are shown to be clearly required for adequate interaction with the proposed binding pocket to occur. This would be achieved by bringing the template/downstream region of DNA close to the fingers and/or by shifting the template/primer region toward helix αC in the palm subdomain.

The two electropositive regions around the hydrophobic wall in helix αE likely contribute to a unique binding mode, providing positively charged beds to both the template and downstream phosphates, and a hydrophobic bed to the bases in the gapped region. The observation that helix αE shows the greatest concentration of perturbations upon DNA binding (Fig. 2*c*) supports this prediction. The conformational adjustments required for DNA to interact with the electropositive pocket of Pol X could contribute to mismatch specificity (low fidelity synthesis) by creating a larger space for a bulky, nascent base pair or positioning the templating base such that it would be sterically and electronically complementary to a 'mismatched' incoming nucleotide. Such a DNA binding-based mechanism for generating mismatch specificity is an alternative, or perhaps additive, approach to the direct nucleotide recognition-based approach suggested in the adjoining paper by Maciejewski *et al.*[17]

A potential multienzyme mutator

High fidelity DNA polymerases are known to enhance the relatively modest selectivity inherent in Watson-Crick base pairing[18] of ~10–100 by imposing additional constraints on the nascent base pair. It has been suggested that low fidelity polymerases do not impose these additional selectivity constraints and that the relatively meager selectivity of base pairing thus becomes the primary fidelity mechanism. However, the fidelity of Pol X is lower than that dictated by Watson-Crick base pairing for at least one mismatched pair (G-G)[1]; thus, the enzyme must be actively involved in overcoming the selectivity imposed by

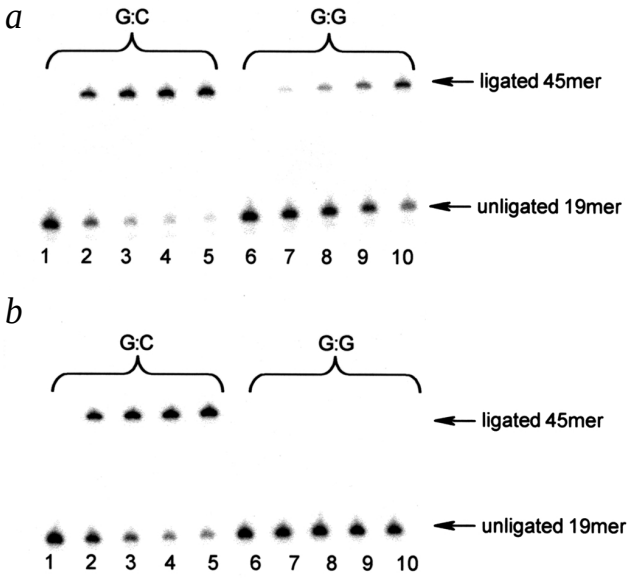

Fig. 4 Fidelity of ASFV DNA ligase. Denaturing polyacrylamide gel of ligation reactions containing 12 pmol of nicked DNA that has a 3′ OH G-C base pair and ***a***, 0 (lane 1), 2.5 (lane 2), 5 (lane 3), 10 (lane 4) or 20 pmol (lane 5) of ASFV ligase. Lanes 6–10 show the equivalent ligation reactions with nicked DNA containing a 3′ OH G-G base pair. ***b***, Same as (*a*) with 0, 10, 20, 40 and 80 fmol of T4 ligase.

Watson-Crick base pairing, probably requiring tight binding and constraint of substrates in a unique alignment (as discussed above). The facts that Pol X is specific at the level of nucleotide binding (for example, 35 μM $K_{d,app}$ for dGTP in the G-G base pair *versus* 260 μM $K_{d,app}$ for dCTP in the G-C base pair[1]) and DNA binding (gapped *versus* nongapped[1]), and that it possesses the ability to bind DNA very tightly support the contention that low fidelity synthesis is at least partially the product of redirected substrate specificity rather than simply relaxed specificity.

The structural and functional analyses support the prediction that Pol X is a strategic DNA mutase (instead of a poor polymerase) that operates in a 'deviant' BER pathway[1]. In such a scenario, DNA repair by ASFV gives rise to a rapid emergence of variants, enabling the rise of mutant strains that can survive a hostile environment. This would be similar to the manner in which the moderate fidelity of human immunodeficiency virus (HIV) reverse transcriptase rapidly produces variants that are resistant to growth-inhibiting drugs. One difference between the strategy utilized by HIV and that proposed for ASFV is that reverse transcriptase is a replicase/mutase (high activity/processivity and moderate fidelity), whereas Pol X is a dedicated DNA mutase (low activity/processivity and extremely low fidelity).

A logical conclusion of the mutagenic BER hypothesis is that the error-prone polymerization activity of Pol X would necessarily be associated with a ligase activity that is capable of sealing nicks that contain a base pair mismatch at the 3′ OH side. Pol β functions in concert with mammalian DNA ligases I and III in the two major mammalian BER pathways[19–21]. Thus, comparison of the 3′ mismatch tolerances of mammalian ligase I or III with the sole ASFV DNA ligase[22] is an additional indicator of the 'mutagenic intent' of the repair pathways in which Pol β and Pol X participate.

To this end, we cloned, overexpressed and purified ASFV ligase and investigated its selectivity in sealing a 3′ G-C *versus* a 3′ G-G containing nick. ASFV ligase is capable of sealing a G-G mismatch-containing nick at ~10% of the efficiency at which it seals the corresponding G-C containing nick (Fig. 4*a*). Within

Table 1 Structural statistics for the Pol X structures[1]

	<SA>	$(\overline{SA})_r$
R.m.s. deviation from experimental distance restraints[2] (Å)		
All (2,353)	0.016 ± 0.001	0.016
Sequential (|I – j| = 1) (602)	0.012 ± 0.001	0.012
Medium range (1 < |I – j| < 5) (420)	0.017 ± 0.001	0.017
Long range (|I – j| > 5) (765)	0.019 ± 0.001	0.018
Intraresidue (454)	0.013 ± 0.001	0.013
Hydrogen bonds (112)	0.020 ± 0.001	0.021
R.m.s. deviation from backbone torsion angle restraints[3] (°) (244)	1.937 ± 0.025	1.926
R.m.s. deviation from idealized geometry		
Bonds (Å)	0.0017 ± 0.00005	0.0017
Angles (°)	0.371 ± 0.003	0.369
Impropers (°)	0.258 ± 0.004	0.263
Measures of structure quality		
E_{L-J}[4] (kcal mol^{-1})	–584 ± 14	–553
PROCHECK analysis[5]		
Most favored regions from Ramachandran plot (%)	82.2 ± 1.3	81.6
Number of bad contacts per 100 residues	7 ± 2	5
Coordinate precision[6] (Å)		
Backbone atoms	0.46 ± 0.05	
All heavy atoms	0.98 ± 0.05	

[1]<SA> are the final 20 simulated annealing structures, $\overline{SA}$ is the mean structure obtained by averaging the coordinates of the individua SA structures best fit to each other, and $(\overline{SA})_r$ is the restrained minimized mean structure. The number of restraints is given in parentheses.
[2]None of the <SA> structures exhibited distance violations >0.3 Å.
[3]The backbone torsion angle (φ and ψ) restraints were derived by using TALOS[31].
[4]E_{L-J} is the Lennard-Jones van der Waals energy calculated with the X-PLOR PARMALLH6 protein parameters[30] and is not included in the target function for simulated annealing or restrained minimization.
[5]Ref. 32.
[6]The coordinate precision of <SA> is defined as the average atomic r.m.s. differences from the mean ($\overline{SA}$) structure.

the ATP-dependent DNA ligase family, mammalian ligases I and III have been shown to discriminate fairly strongly against 3′ OH mismatches (particularly 3′ purine-purine mismatches)[23], whereas T4 bacteriophage ligase has been described as an example of broad substrate tolerance[24], based on relatively weak discrimination against at least some 3′ OH mismatches[24,25]. However, even T4 ligase discriminates against the 3′ OH G-G mismatch more effectively than does ASFV ligase (Fig. 4*b*), highlighting the unique nature of the relaxed specificity of the ASFV ligase against this mismatch. The unusual tolerance of ASFV ligase toward a 3′ OH G-G mismatch supports the hypothesis of a mutagenic viral BER pathway that is initiated by low fidelity nucleotide incorporation catalyzed by ASFV Pol X and consummated by low fidelity nick-ligation catalyzed by ASFV ligase.

Methods

Sample preparation. Pol X samples were prepared as described[1], except in the absence of glycerol for NMR samples. Uniformly $^{13}C/^{15}N$- and ^{15}N-labeled proteins were prepared by growing *Escherichia coli* in M9 medium containing $^{15}NH_4Cl$ with and without $^{13}C_6$-glucose, respectively. ASFV ligase was subcloned from pLD20 (containing an ASFV genomic fragment) into pET-17b (Strategene), expressed and purified under conditions identical to those used for Pol X[1], with the exception that induction was at 25 °C. DNA substrates were ordered from Integrated DNA Technologies or synthesized on a Perkin-Elmer 392 synthesizer and purified by denaturing PAGE as described[1].

NMR spectroscopy. NMR experiments were performed on a Bruker DMX-600 or DRX-800 spectrometer at 20 °C. The NMR samples contained 0.5–1 mM Pol X, 50 mM borate, 50 mM KCl, 1 mM DTT and 1 mM EDTA in 95% (v/v) H_2O/5% D_2O or 100% D_2O, pH 7.5. Total resonance (^1H, ^{15}N and ^{13}C) assignments were obtained using 3D HNCA, HN(CO)CA, HNCO, HCACO, HNCACB, CBCA(CO)NH, HCCH-TOCSY, ^{15}N-edited TOCSY and NOESY, and ^{13}C-edited NOESY experiments[26,27]. Aromatic side chain resonance assignments were obtained using 2D NOESY and TOCSY. The NMR data were processed using XWIN-NMR 2.6 (Bruker).

DNA binding by Pol X was monitored with 2D ^{15}N-HSQC spectra[28] on uniformly ^{15}N-labeled protein samples with varying concentrations of added DNA. DNA sequence was identical to that used for crystallographic studies of Pol β[16]. Buffer was identical to that described above except that KCl was at 500 mM, and 10 mM $MgCl_2$ was added.

Structural calculations. NMR structures were calculated using a simulated annealing method[29] within X-PLOR (version 3.843)[30]. Distance restraints were obtained from 2D NOESY and 3D ^{15}N-edited and ^{13}C-edited NOESY experiments (mixing time of 100 ms). Backbone torsion angle restraints were obtained by using TALOS[31] in which ^{15}N, ^1HN, $^{13}C\alpha$, $^1H\alpha$, $^{13}C\beta$ and $^{13}C'$ chemical shift values of Pol X were used as input to generate the restraints. Structures were refined using an iterative process in which the structures of one generation were used to resolve ambiguous NOE assignments, which in turn were included in the structure calculation of the next generation. The structures were analyzed by X-PLOR[30], PROCHECK[32] and MOLMOL[33]. All structure figures were generated with MOLMOL.

DNA binding assays. Band shift analysis was performed as described[7], but with the following exceptions: solvent was the same as used for NMR binding experiments, [DNA] was 1 μM and a two-step gradient gel of 4%, 20% and 25% acrylamide was used. For $K_{d,DNA}$ measurements, 20 nM polymerase was preincubated with 5, 10, 20, 40, 80 or 160 nM gapped DNA prior to reaction initiation. Burst amplitudes were determined by fitting to the burst equation: $[26mer] = A(1 - e^{-k_{-1}t}) + (k_{ss} \times t)$. The burst amplitude (A) was then plotted as a function of DNA concentration and the resulting plot fit to the quadratic equation: $A = 0.5([E]_0 + [D]_0 - K_{d,DNA}) - (0.25([E]_0 + [D]_0 + K_{d,DNA})^2 - [E]_0[D]_0)^{1/2}$. For the competition experiment, 300 nM Pol X and 300 nM Pol β were preincubated with 200 nM gapped DNA prior to reaction initiation. The resulting turnover was fit to the double exponential equation: $[26mer] = A^{\beta}(1 - e^{-kt}) + A^{X}(1 - e^{-kt})$. Reaction conditions and product formation analysis were as described[1].

Ligase Assay. Nicked DNA substrate preparation was as described[1] for the gapped DNA substrate, with the exception that 19mer 'downstream' oligonucleotide, rather than primer, was radiolabeled and that the primer was one nucleotide longer (dCMP or dGMP) at the 3′ terminus. A solution containing 200 nM nicked DNA was mixed with a solution containing 200 μg ml^{-1} BSA, varying amounts of ligase, 2 mM ATP and 20 mM DTT, and incubated at 37 °C for 15 min prior to quenching with an equivalent volume of 0.6 M EDTA, pH 8.0. PAGE analysis of turnover was as described[1]. Ligase amount was estimated by A_{280} and is subject to error; however, the relative amounts within each gel are accurate.

Coordinates. Coordinates have been deposited in the Protein Data Bank (accession code 1JQR).

Acknowledgments

We thank C. Yuan for assistance in initial NMR experiments and L. Dixon for her gift of the plasmid pLD20 containing an ASFV genomic fragment that included locus NP419L. R. Coleman and R. Perez assisted in the preparation of DNA. This work was supported by a grant from the National Institutes of Health.

Correspondence should be addressed to I.-J.L.B. *email: byeon.2@osu.edu* or M.-D.T. *email: tsai.7@osu.edu*

Received 27 June, 2001; accepted 13 September, 2001.

1. Showalter, A.K. & Tsai, M.-D. *J. Am. Chem. Soc.* **123**, 1776–1777 (2001).
2. Sobol, R.W. *et al. Nature* **379**, 183–186 (1996).
3. Yañez, R.J. *et al. Virology* **208**, 249–278 (1995).
4. Oliveros, M. *et al. J. Biol. Chem.* **272**, 30899–30910 (1997).
5. Sawaya, M.R., Pelletier, H., Kumar, A., Wilson, S.H. & Kraut, J. *Science* **264**, 1930–1935 (1994).
6. Steitz, T.A. *J. Biol. Chem.* **274**, 17395–17398 (1999).
7. Kraynov, V.S., Showalter, A.K., Liu, J., Zhong, X. & Tsai, M.-D. *Biochemistry* **39**, 16008–16015 (2000).
8. Steitz, T.A., Smerdon, S.J., Jager, J. & Joyce, C.M. *Science* **266**, 2022–2025 (1994).
9. Holm, L. & Sander, C. *Trends Biochem. Sci.* **20**, 478–480 (1995).
10. Pelletier, H., Sawaya, M.R., Kumar, A., Wilson, S.H. & Kraut, J. *Science* **264**, 1891–1903 (1994).
11. Wishart, D.S., Bigam, C.G., Holm, A., Hodges, R.S. & Sykes, B.D. *J. Biomol. NMR* **5**, 67–81 (1995).
12. Senkevich, T.G., White, C.L., Koonin, E.V. & Moss, B. *Proc. Natl. Acad. Sci. USA* **97**, 12068–12073 (2000).
13. Doublié, S., Tabor, S., Long, A.M., Richardson, C.C. & Ellenberger, T. *Nature* **391**, 251–258 (1998).
14. Najmudin, S. *et al. J. Mol. Biol.* **296**, 613–632 (2000).
15. Casas-Finet, J.R., Kumar, A., Karpel, R.L. & Wilson, S.H. *Biochemistry* **31**, 10272–10280 (1992).
16. Sawaya, M.R., Prasad, R., Wilson, S.H., Kraut, J. & Pelletier, H. *Biochemistry* **36**, 11205–11215 (1997).
17. Maciejewski, M.W. *et al. Nature Struct. Biol.* **8**, 936–941 (2001).
18. Loeb, L.A. & Kunkel, T.A. *Annu. Rev. Biochem.* **51**, 429–457 (1982).
19. Prasad, R. *et al. J. Biol. Chem.* **271**, 16000–16007 (1996).
20. Nash, R.A., Caldecott, K.W., Barnes, D.E. & Lindahl, T. *Biochemistry* **36**, 5207–5211 (1997).
21. Cappelli, E. *et al. J. Biol. Chem.* **272**, 23970–23975 (1997).
22. Hammond, J.M., Shona, M.K., Smith, G.L. & Dixon, L.K. *Nucleic Acids Res.* **20**, 2667–2671 (1992).
23. Husain, I. *et al. J. Biol. Chem.* **270**, 9683–9690 (1995).
24. Tong, J., Cao, W. & Barany, F. *Nucleic Acids Res.* **27**, 788–794 (1999).
25. Wu, D.Y. & Wallace, R.B. *Gene* **76**, 245–254 (1989).
26. Bax, A. & Grzesiek, S. *Acc. Chem. Res.* **26**, 131–138 (1993).
27. Clore, G.M. & Gronenborn, A.M. *Biol. Magn. Reson.* **16**, 3–26 (1998).
28. Grzesiek, S. & Bax, A. *J. Am. Chem. Soc.* **115**, 12593–12594 (1993).
29. Nilges, M., Clore, G.M. & Gronenborn, A.M. *FEBS Lett.* **239**, 129–136 (1988).
30. Brunger, A.T. X-PLOR. *A system for X-ray crystallography and NMR. 3.1 edn* (Yale University, New Haven; 1992).
31. Cornilescu, G., Delaglio, F. & Bax, A. *J. Biomol. NMR* **13**, 289–302 (1999).
32. Laskowski, R.A., MacArthur, M.W., Moss, D.S. & Thornton, J.M. *J. Appl. Crystallogr.* **26**, 283–291 (1993).
33. Koradi, R., Billeter, M. & Wuethrich, K. *J. Mol. Graphics* **14**, 51–55 (1996).